REPORT DOCUMENTATION PAGE

AFRL-SR-AR-TR-04-

0520

1. REPORT DATE *(DD-MM-YYYY)*	2. REPORT TYPE	3. DATES COVERED *(From - To)*
	Final Report	01 Jul 2003 - 14 May 2004

4. TITLE AND SUBTITLE	5a. CONTRACT NUMBER
Continuum Modeling of Nanotube Composites	
	5b. GRANT NUMBER
	F49620-03-1-0385
	5c. PROGRAM ELEMENT NUMBER

6. AUTHOR(S)	5d. PROJECT NUMBER
Dr. Frederick Bloom	
	5e. TASK NUMBER
	5f. WORK UNIT NUMBER

7. PERFORMING ORGANIZATION NAME(S) AND ADDRESS(ES)	8. PERFORMING ORGANIZATION REPORT NUMBER
Department of Mathematical Sciences Northern Illinois University DeKalb IL 60115	

9. SPONSORING/MONITORING AGENCY NAME(S) AND ADDRESS(ES)	10. SPONSOR/MONITOR'S ACRONYM(S)
USAF/AFRL AFOSR 801 N. Randolph Street Arlington VA 222003	AFOSR
	11. SPONSOR/MONITOR'S REPORT NUMBER(S)

12. DISTRIBUTION/AVAILABILITY STATEMENT

Distribution Statement A. Approved for public release; distribution is unlimited.

13. SUPPLEMENTARY NOTES

14. ABSTRACT

The authors present a critical analysis of the recent literature related to modeling the continuum mechanical behavior of carbon nanotubes; they also describe a methodology based on combining molecular dynamics simulations, equivalent continua modeling, and mathematical homogenization theory which is directed at obtaining the constitutive relations that can be used to model a nanotube as an elastic cylindrical shell.

20041028 036

15. SUBJECT TERMS

16. SECURITY CLASSIFICATION OF:			17. LIMITATION OF ABSTRACT	18. NUMBER OF PAGES	19a. NAME OF RESPONSIBLE PERSON
a. REPORT	b. ABSTRACT	c. THIS PAGE			
U	U	U	UU	15	19b. TELEPHONE NUMBER *(Include area code)*

Standard Form 298 (Rev. 8/98)
Prescribed by ANSI Std. Z39.18

Final Report
AFOSR Grant F49620-03-1-0385

Mathematical Modeling of the Continuum
Response of Carbon Nanotubes

Hamid Bellout & Frederick Bloom
Department of Mathematical Sciences
Northern Illinois University
DeKalb, IL 60115

Summary

The authors present a critical analysis of the recent literature related to modeling the continuum mechanical behavior of carbon nanotubes; they also describe a methodology based on combining molecular dynamics simulations, equivalent continua modeling, and mathematical homogenization theory which is directed at obtaining the constitutive relations that can be used to model a nanotube as an elastic cylindrical shell.

I. Background (The Literature Review)

Interest has been generated in nano-structured materials because of their potential for providing significant improvements in both mechanical and physical properties with respect to traditional structural materials. Investigations [1] point to the fact that carbon nanotubes possess a high elastic modulus (in the 1-5 TPa range) and can sustain an elastic strain on the order of 5%; and a fracture strain up to 20%; their strength is, therefore 'unmatched by any other known material' [2]. As indicated in [3] and [4], because small fiber composites are easier to process, the mechanical properties of carbon nanotubes, coupled with their small dimensions and large aspect ratios, make them candidates for the fabrication of the optimal carbon fiber reinforced materials. Work is needed on modeling the constitutive response of single-walled carbon nanotube (SWNT's) and multi-walled carbon nanotubes (MWNT's) in order that reliable constitutive relations can be developed to predict the bulk mechanical properties of nanotube-polymer composites in terms of the molecular structure of the polymer, the nanotubes, and the polymer/nanotube interfaces. As pointed out, in [5], 'in order to implement nanotube-composite design intelligently, it is vital to understand the mechanical behavior of nanotubes.' As the authors of [6] indicate 'even classical molecular dynamics (MD) computations are still limited to simulating on the order of $10^6 - 10^8$ atoms for a few nanoseconds. The simulation of larger systems or longer times must currently be left to continuum methods.' *The effective continuum modeling of carbon nanotubes, the graphene layers of which they are the 'cylindrical' images, and the delineation of the mapping which takes one from the graphene layer to the nanotube surface, as well as the dependence of that mapping on the chirality vector, form one of the central foci of this proposal, the other being the deduction of a set of constitutive relations for the response of nanotube/polymer composites.*

Almost all modeling of the response of carbon nanotubes ([1], [7]-[25]), and irrespective of whether the authors treat the nanotubes as shells (with some 'effective' thickness) or as beams (with some effective 'cross-section'), *assumes that the 'surface' of the 'cylindrical' nanotube exhibits isotropic mechanical response to deformations;* this assumption is based, in turn, on two hypotheses, namely, that

(i) the response of a graphene layer is a consequence of the isotropic behavior of graphite ([26], Chapter 3) in the basal plane (or, alternatively, as argued in [9], that the isotropic response of a graphene sheet is a consequence of the intrinsic hexagonal symmetry of the array of carbon atoms comprising the sheet) and

(ii) that the nanotube can be viewed (e.g., [13]) as a 'conformal mapping of a two dimensional honeycomb lattice to the surface of a cylinder subjected to periodic boundary conditions'

Our research has shown that *neither of hypotheses (i) and (ii) is in accord with the recent literature [6] on MD simulations of the response of carbon nanotubes, or with experimental observations.* Maintaining the isotropy hypothesis for the response of the nanotube in its basal plane has led to *inconsistencies* among the results for the bending stiffness of SWNT's, the representative thickness of nanotubes, and experimental results on in-plane stiffness; these inconsistencies are highlighted in § II. As noted in [6] 'the fundamental assumption of the continuum approximation, that quantities vary slowly over lengths on the order of the atomic scales, breaks down in nano-mechanics.'

Since their discovery there has been an increasing interest in carbon nanotubes because of their novel structure and properties and the wealth of potentially important applications.

As indicated, e.g., in [24], beyond being remarkably stiff and strong, SWNT's are outstanding conductors of electricity and are 'projected to conduct heat even better than diamond.' Under development are SWNT nanodevices and nanocircuits exhibiting superior logic and amplification functions. Because nanotubes are hollow they can be used in sensitive sensor devices as well as in a variety of biomedical applications.

Composite materials based on carbon nanotubes have the potential of providing strength-to-weight ratios which exceed those of any materials currently available, in part because aspect ratios for nanotube fibers of well over 1000 are realizable. As indicated in, e.g., [35], 'in contrast to standard carbon fibers nanotubes remain curved and interwoven in the composite suggesting extreme flexibility.' Effective utilization of nanotubes in composites depends on the ability to disperse the nanotubes homogeneously throughout the matrix (without destroying their integrity). Also, there must be good interfacial bonding between the nanotubes and the polymer to achieve load transfer across the nanotube-matrix interface; the vehicle for such load transfer is the interfacial shear stress. Provided the load can be effectively transferred to the nanotube, the modulus of the composite is conjectured to be that of randomly oriented short fiber composites containing fibers of extremely high modulus and strength. Nanotube composites can be modeled by standard techniques in the theory of heterogeneous materials (e.g., [36] or [37]), or would themselves become a suitable object to which to apply homogenization techniques, *a prerequisite for either approach is a firm understanding of the continuum mechanical behavior of an individual nanotube.* The same considerations apply when one considers MWNT's as potential reinforcing agents; in this case the strength of the composite is also affected by the ease with which individual nanotubes slide with respect to each other. In a MWNT the outer nanotube is loaded but, because of the relatively weak bonding between nanotube layers, the load in not transferred to the inner tubes if they slip with respect to the outertubes; the interactions between SWNT's in a bundle is similar to the interlayer interactions of MWNT's and, as pointed out in [38], slippage within bundles can easily occur. *An effective continuum model for the mechanical response of MWNT's depends on having such a model for SWNT's.*

A graphene sheet is a honeycomb lattice of carbon atoms in a hexagonal array as depicted in fig. 1. In terms of base vectors $\boldsymbol{a}_1, \boldsymbol{a}_2$ the nanotube chirality vector $\boldsymbol{r} = n\boldsymbol{a}_1 + m\boldsymbol{a}_2$ where n, m are integers with $0 \leq |m| < n$. The chiral angle θ is formed by $\boldsymbol{r}$ and $\boldsymbol{a}_1$. An (n, m) nanotube is constructed by using $\boldsymbol{r}$ as a 'roll-up' vector, so that with respect to the crystallographically equivalent sites A, A', B, and B' ($\boldsymbol{t} = \vec{OB}$ is the direction of the nanotube axis) A and A' coincide as do points B and B'. The rectangle $AA'B'B$ defines the unit cell for the nanotube. The basic SWNT structures conform to chiral vectors of type $(n, 0)$ [zig-zag nanotubes] and type (n, n) [armchair nanotubes]. The rolled-up unit cell is capped by one half of a C_{60} molecule. Most nanotubes do not exhibit the highly symmetric forms associated with zig-zag and armchair nanotubes but, rather, have structures in which the 'hexagons' are arranged helically around the tube axis (chiral nanotubes). *'Hexagons' lying on the idealized nanotube surface may be deformed versions of those which form the graphitic sheet,* e.g., as indicated in [12], with reference to the C-C bonds on the nanotube surface, 'the angles between these bonds depend on the radius of the cylinder as well as on their orientations ... all angles approach 120° (the value in a perfect graphitic plane) with increasing cylindrical radius. *For tubules with smaller radii, for example, the bond angles deviate up to 9% from their planar value.'* Moreover, 'upon forming curved surfaces for tubules, the nearest neighbor C-C distances change depending on their relative orientations with respect to the cylindrical axis direction.' Statements in, e.g., [13] which point to the nanotube surface as being 'a conformal mapping

2

of a two-dimensional honeycomb lattice' *do not accurately depict the deformation which leads from a unit cell of the graphitic sheet to its image on the surface of the (idealized) cylindrical nanotube.* Many authors have suggested using the elastic moduli of graphite for SWNT's by neglecting the change in structure that occurs when a graphene sheet is rolled into a nanotube but recent work [6] has emphasized that 'the *deformation is, in fact, not homogeneous as the graphene sheet is rolled into (a carbon nanotube) ... the energy of the (carbon nanotube) not only depends on the deformation gradient but also depends on higher-order derivatives of (the deformation gradient). In such a case, a set of high(er)-order elastic constants that belongs to the framework of multipolar theory needs to be determined.'* Multipolar continuum models have been considered by the authors in [39]-[44]. Thus, *even if we could justify modeling the graphitic sheet as an isotropic elastic continuum one can not carry isotropic response over to the nanotube surface* and recent molecular dynamics simulations (based on Brenner's potential [45]) have been reported by the authors of [6] which lead to a prediction of anisotropic behavior in the basal plane of a nanotube surface.

Other arguments support the hypothesis that the response of the nanotube surface is not that an elastic isotropic material. *If the graphitic sheet can be considered to be an isotropic elastic continuum, whose conformal image is the nanotube surface, then the response of the nanotube should be independent of chirality:* as we roll up a unit cell the graphitic sheet the response of the resulting structure (SWNT) should be independent of the orientation of the edge of the cell with respect to the lattice vector a_1; this is not the case, e.g., if one 'rolls up' an arbitrarily oriented rectangular subset of a sheet of rectilinearly orthotropic material, such as paper, into a cylinder (as as been demonstrated by the authors in [46]). Chirality independence has been claimed by several authors, e.g., [9] asserts that *because of the hexagonal symmetry of a graphite sheet its elastic properties are two-dimensionally isotropic, and so the helicity of the tube plays no significant role"* and Lu [8] announced results for carbon nanotubes which are independent of both tube size and chirality. However, it was noted in [19], that *'the apparent insensibility of the Young's modulus on the tube size and chirality observed by Lu is due to the fact that an empirical pair potential was used in his calculations, and such a model will not reflect the effects that the curvature will have on the bonding properties of the system.'* The observations made in [19] have appeared in other recent references, e.g., Yao and Lordi [18] observe that 'for a nanotube of small radius, *Young's modulus depends on the radius and helicity of the tube owing to changes in bonding that effect the torsional strain;'* such changes in bonding are directly related to the nonhomogeneity of the map from the graphene sheet to the surface of the nanotube. The failure to include torsional strain contributions in MD simulations of nanotube behavior explains why earlier calculations 'did not reveal significant effects of helicity on elastic properties.' In fact it was noted in [47] that *'the strain energy under large strain conditions shows significant sensitivity to helicity'* while Zhao, et. al. [2] note that *'the behavior of nanotubes under large tensile strain depends strongly on their symmetry and diameter ... different orientations of the carbon bonds with respect to the strain axis in tubes of different symmetry lead to completely different scenarios.'*

One additional set of results mitigate against modeling a SWNT as an elastic shell which is isotropic in its basal plane, namely, *those results which relate Young's modulus, bending stiffness, and in-plane stiffness.* Most authors use the equilibrium interlayer spacing between adjacent nanotubes ($h = 0.34$nm) as the effective thickness of SWNT's. However, Yakobson, et.al., [9] report an in-plane stiffness for a SWNT of $C = 59eV/atom = 360J/m^2$ and a flexural rigidity of $D = 0.85eV$, as well as a Poisson ration of $\nu = 0.19$; if one uses these measured values *in conjunction with the standard relations associated with an 'isotropic' shell,* i.e, $D =$

$Yh^3/12(1-\nu^2)$ and $C = Yh$ then $h = 0.066$ nm while the Young's modulus $Y = 5.5TPa$. The value of $h = 0.066$ nm obtained is actually smaller than the typical C-C bond length in the graphitic sheet while the value of $Y = 5.5TPa$ is several times higher that the usually quoted range of $1 - 2TPa$. However, if (as Ru [24] points out) one begins with a value of $Y = 1.1TPa$ (consistent with $h = 0.34$nm and $C = 360J/m^2$) and substitutes these values into the above expression for D, a computed D is obtained which is 25 times larger than the measured value of $D = 0.85eV$. These inconsistencies are a consequence of assuming that the nanotube is isotropic in its basal plane. For a cylindrical shell which is the image of a rectilinearly orthotropic sheet one obtains (Bellout and Bloom [46], Bloom and Coffin [48]) for the in-plane principal bending stiffnesses $D_1 = Yh^3/12(1 - (\nu/\gamma)^2)$ and $D_2 = \gamma^2 Yh^3/12(1 - (\nu/\gamma)^2)$ which are equal if and only if the orthotropic ratio $\gamma = c_{22}/c_{11} = 1$ where c_{11} and c_{22} are, respectively, the (in-plane) elastic constants in the axial and radial directions. The construction of a continuum model for the response of a nanotube should not depend on the a priori assumption of basal plane isotropic response and should (i) resolve the inconsistencies with respect to the measured data for Y and C and the values of effective shell thickness h and (ii) provide a basis for the formulation of realistic constitutive relations for nanotube/polymer composites.

II A Continuum Approach to Nanotube Modelling

In this section we detail an approach to the continuum modeling of single-walled nanotubes; this approach is based on homogenization theory.

Homogenization theory relates to structures that have two naturally associated length scales, a 'micro-scale' l and and macroscale L; the physical properties of the medium vary rapidly on the scale l and more slowly on the larger scale L. The ratio $\epsilon = l/L$ plays a key role wherein it is assumed that every property of the medium is of the form $\boldsymbol{F}(\boldsymbol{x}, \boldsymbol{y})$ with $\boldsymbol{x}$ the position vector of a point in the medium and $\boldsymbol{y} = \boldsymbol{x}/\epsilon$ the vector of stretched coordinates. It is usually the case that the microstructure is periodic (which is reflected in the periodicity of $\boldsymbol{F}(\boldsymbol{x}, \boldsymbol{y})$ with respect to $\boldsymbol{y}$); this is the case for the graphitic sheet by virtual of the hexagonal symmetry displayed in fig. 1. For the graphitic sheet $\boldsymbol{x} = (x_1, x_2)$, $\boldsymbol{y} = (x_1/\epsilon, x_2/\epsilon)$ but in its (flat) undeformed state physical properties depend only on $\boldsymbol{y}$, i.e., $\boldsymbol{F} = \boldsymbol{F}(\boldsymbol{y})$.

In homogenization theory each field quantity $\boldsymbol{u}^\epsilon(\boldsymbol{x}) = \boldsymbol{u}(\boldsymbol{x}, \boldsymbol{x}/\epsilon)$ is conceived of as having a double-scale asymptotic expansion of the form

$$\boldsymbol{u}^\epsilon(\boldsymbol{x}) = \boldsymbol{u}^\circ(\boldsymbol{x}, \boldsymbol{y}) + \epsilon\boldsymbol{u}^1(\boldsymbol{x}, \boldsymbol{y}) + \epsilon^2\boldsymbol{u}^2(\boldsymbol{x}, \boldsymbol{y}) + \cdots \qquad (1)$$

Each of the terms $\boldsymbol{u}^i(\boldsymbol{x}, \boldsymbol{y})$ is periodic in $\boldsymbol{y}$ with the same period as the structure in question; the ansatz (1) yields, in many cases, a rigorous procedure for deducing macroscopic equations, in $\boldsymbol{x}$, for the overall behavior of the medium.

In the situation we are interested in the global macroscopic behavior is reflected in a set of homogenized elastic constants a_{ij}^h which mediate the elastic response of a graphitic sheet at the continuum level. At the microscopic level the mechanical response of the graphitic sheet will be governed by a conservation law of the form

$$-\frac{\partial}{\partial x_i}\left(a_{ij}^\epsilon(\boldsymbol{x})\frac{\partial\boldsymbol{u}^\epsilon}{\partial x_j}\right) = \boldsymbol{f}^\epsilon \qquad (2)$$

4

where the $a_{ij}^\epsilon(x) = a_{ij}(x, \frac{x}{\epsilon})$ are periodic in y with period Y, i.e., $a_{ij}(x, y) = a_{ij}(x, y + Y)$ and satisfy $a_{ij}^\epsilon = a_{ji}^\epsilon$, $a_{ik}^\epsilon \xi_i \xi_k \geq \gamma \xi_j \xi_j, \gamma > 0$. The period Y serves to define a unit cell Y and will be defined, below, for the graphitic sheet; ϵ *and* Y *for our problem must be chosen so as to reflect a distinct dependence on the magnitude of the chirality vector as well as on the chiral angle.* The (microscale) forcing function f^ϵ is also assumed to be Y periodic in y.

The basic idea in the homogenization scheme is to substitute the expansion (1) into (2) and then identify powers of ϵ; using the fact that

$$\frac{\partial}{\partial x_j}\phi(x, x/\epsilon) = \left(\frac{\partial \phi}{\partial x_j} + \frac{1}{\epsilon}\frac{\partial \phi}{\partial y_j}\right) \tag{3}$$

this procedure yields, at order $O(\epsilon^{-2})$,

$$\frac{\partial}{\partial y_i}(a_{ij}\frac{\partial u^o}{\partial y_j}) = 0 \tag{4}$$

an equation for the Y periodic function $u^o(x, y)$ whose only solution is $u^o(x, y) \equiv u^o(x)$. At order $O(\epsilon^{-1})$, assuming $u^o(x)$ is known, we obtain for u^1 the following elliptic equation in a unit cell Y whose solution must satisfy Y periodicity:

$$\frac{\partial}{\partial y_i}\left(a_{ij}\left[\frac{\partial u^1}{\partial y_j} + \frac{\partial u^o}{\partial x_j}\right]\right) = 0. \tag{5}$$

It may be shown (see [27], [28]) that u^1 can be expressed in the form

$$u^1(x, y) = \frac{\partial u^o}{\partial x_k}w_k + \hat{u}^1(x) \tag{6}$$

where $\hat{u}^1(x)$ is an arbitrary function of x representing the mean value of $u^1(x, y)$ on Y and $w_k \in W_Y = \{\phi \in H^1(Y) | \phi \text{ is } Y\text{periodic and } \hat{\phi} = \frac{1}{|Y|}\int_Y \phi(y)dy = 0\}$ is *the unique solution of the variational equation*

$$\int_Y a_{ij}\frac{\partial w_k}{\partial y_j}\frac{\partial \phi}{\partial y_i}dy = -\int_Y a_{ik}\frac{\partial \phi}{\partial y_i}dy, \forall \phi \in W_Y. \tag{7}$$

If we write (2) in divergence form (in terms of the Cauchy stress tensor t) as

$$-\operatorname{div} t^\epsilon = f^\epsilon \text{ with } t_{ik}^\epsilon = a_{ij}^\epsilon\frac{\partial u_k^\epsilon}{\partial x_j} \tag{8}$$

expand t^ϵ as $t^\epsilon(x) = t^o(x, y) + \epsilon t^1(x, y) + \cdots$, substitute into the expression for t^ϵ the expansion (1) for $u^\epsilon(x)$, and then set $\epsilon = 0$, we obtain

$$t_{ik}^o(x, y) = a_{ij}\left(\frac{\partial u_k^o}{\partial x_j} + \frac{\partial u_k^1}{\partial y_j}\right). \tag{9}$$

The integral form of the conservation law in (8), *in a macroscopic domain D, composed of whole periods,* is, $-\int_{\partial D} t^\epsilon \cdot n dS = \int_D f^\epsilon dV$ which, to first order in ϵ yields

$$-\int_{\partial D} \hat{t}^o \cdot n dS_x = \int_D \hat{f}dx \tag{10}$$

5

From (10) we obtain the *macroscopic equations*

$$- \operatorname{div} \hat{\boldsymbol{t}}^0 = \hat{f} \text{ with } \hat{t}_{ij}^o = a_{ik}^h \frac{\partial u_j^o}{\partial x_k} \tag{11}$$

where the *homogenized coefficients (elastic constants)* a_{ik}^h *are given by*

$$a_{ik}^h(\boldsymbol{x}) = \frac{1}{|Y|} \int_Y (a_{ik} + a_{ij} \frac{\partial w_k}{\partial y_i}) dy. \tag{12}$$

If the original coefficients $a_{ij} = a_{ij}(\boldsymbol{y})$ are independent of $\boldsymbol{x}$ then the a_{ij}^h's are constants; *this will be the case for homogenization of a graphitic sheet because of the strict periodicity of the 'micro' (atomistic) structure.* We observe that the *homogenized medium may be anisotropic even if its behavior at the microstructure level is isotropic:* even if $a_{ij} = a\delta_{ij}$, (12) implies that

$$a_{ik}^h = \frac{1}{|Y|} \int_Y a \frac{\partial w_k}{\partial y_i} dy \tag{13}$$

in which case it *does not necessarily follow that* $a_{ik}^h = 0$ for $i \neq k$. This observation is of central importance for the (homogenized) macroscopic behavior of a graphitic sheet.

To apply homogenization theory to a 'nanotube unit cell', in an undeformed graphitic sheet, we now identify both the microscale unit cell Y and the elasticity coefficients $a_{ij}(\boldsymbol{x}, \boldsymbol{y})$ which appear in (12).

In fig. 2a we depict one 'hexagonal' array of carbon atoms in the unit cell $AA'B'B$ shown in fig. 1. We have located the vertex at which the bravis lattice vectors $\boldsymbol{a}_1, \boldsymbol{a}_2$ originate at the point $(0,0)$ in the x, y plane. The chiral angle for the array from which this 'hexagon' has been selected is θ and the chirality vector $\boldsymbol{r}$ has components (n, m) with respect to the basis vectors $\boldsymbol{a}_1, \boldsymbol{a}_2$; the 'hexagon' is shown as having a 'banded' structure with domain Y_1 being an idealized rectilinear domain of width λ. In Y_1 non-zero elastic constants are generated by the forces associated with C-C bonding; these forces are modeled by molecular dynamics simulations. In the 'interior' of the 'hexagon' the elastic constants on the microscale are taken to be zero. We note that (i) *the assumption that the arrays of carbon atoms in the graphitic lattice are perfect 'hexagons' is a mathematical idealization only, (ii) the band width λ is not well-defined and may be chosen to be a parameter in the model, and (iii) the curves bounding the domain Y_1 need not be rectilinear but may be idealized to be so in a first model.*

To make clear the dependence of the homogenized coefficients a_{ij}^h on both the chiral angle θ and the magnitude $\sqrt{m^2 + n^2}$ of the chirality vector $\boldsymbol{r}$ we proceed as follows: (i) rotate the banded hexagon in fig. 2a. θ radians counterclockwise so that the rotated lattice vector $\boldsymbol{a}_1$, i.e. $\boldsymbol{a}_1'$ in fig. 2b, is in the direction of the chirality vector $\boldsymbol{r}$, (ii) identify the vector of periodicity as being $\boldsymbol{a}_2'$, select for the microscale measure the length l of the line segment $\overline{OA}$ in fig. 2a., (iii) choose $\epsilon = l/\sqrt{m^2 + n^2}$, and (iv) define the domain of integration in (13) to be $Y \equiv Y_\theta = Y_1^\theta \cup Y_2^\theta$ where the $Y_i^\theta, i = 1, 2$, as shown in fig. 2b are the rotated images of the planar domains $Y_i, i = 1, 2$ of fig. 2a. In the present situation (undeformed lattice) the molecular level $a_{ij}(\boldsymbol{y})$ are of the form

$$a_{ij}(\boldsymbol{y}) = \begin{cases} \bar{a}_{ij}(\boldsymbol{y}), & \boldsymbol{y} \in Y_1^\theta \\ 0, & \boldsymbol{y} \in Y_2^\theta \end{cases} \tag{14}$$

While the $a_{ij}(\boldsymbol{y})$ may appear to be discontinuous along the boundary between Y_1^θ and Y_2^θ one

6

may always introduce standard 'cut-off' functions so as to effect a smooth transition from Y_1^θ to Y_2^θ.

The remaining issue is the specification of the $\bar{a}_{ij}(\boldsymbol{y})$ in (15); these are obtained from MD simulations ([49], [50] or [51]) of the energy associated with the C-C bonding in graphitic sheets. The total energy associated with a typical C-C bond has the form

$$E = E_R + E_\theta + E_\emptyset + E_\omega + E_{vdW} + E_{el} \tag{15}$$

where E_R is associated with bond stretching, E_θ with bond angle bending, $E_\emptyset$ with torsion, E_ω with inversions (out-of plane bending), E_{vdW} with Van der Waals interactions, and E_{el} with electrostatic interactions. Our work, to this point has singled out functional forms for each term in (15) which are given, e.g., in [38] and are based on MD simulations; alternative forms for $\boldsymbol{E}$ may be found in [52] which compares the consequences of using either standard 'Brenner' or 'modified Morse' potentials. Employing the Tersoff-Brenner model the review [6] has shown how to *generate the elasticity tensor associated with any particular MD model by treating the energy E as the potential function for a hyperelastic material; we have now determined that such a procedure will serve well to generate the $\bar{a}_{ij}(\boldsymbol{y})$ in (15).* In particular our early work has directed us to focus on the classical Tersoff-Brenner model with associated empirical equation

$$\Phi_{ij} = \Phi_R(r_{ij}) - \overline{B}_{ij}\Phi_A(r_{ij}) \tag{16}$$

in which i, j are indices for neighboring carbon atoms, r_{ij} is the corresponding spatial separation, and Φ_R and Φ_A represent the repulsive and attractive part of the potential, respectively. The effect of bonding angle is included in the term $\overline{B}_{ij}$. The energy density E is then given by

$$E = \Phi/A_o, \;\; \Phi = \sum_{l=1}^{3} \Phi_l \tag{17}$$

where A_o is the area of the undeformed hexagon and Φ_l is the bond energy for the l-th bond. Finally, in terms of the Lagrangian strain tensor e_{ij}, associated with a deformation of the graphene sheet, we will take for the elasticity tensor components

$$c_{ijkl} = \frac{\partial^2 E}{\partial e_{ij}\,\partial e_{kl}}$$

which, because of the symmetries with respect to interchange of indices, serves to generate the $\bar{a}_{ij}$ in (14).

As the graphene sheet is 'rolled up' into a nanotube, the hexagonal array in the unit cell $AA'B'B$ deforms (fig. 3 depicts the different surface arrays for two types of SWNT's); the deformation gradient associated with this mapping (the mapping $f : A \to B$ of fig. 4) is determined, as pointed out in [6], by "the direction and length of the chirality vector and the subsequent mechanical relaxation after rolling." For various configurations of deformed 'hexagonal arrays' on nanotube 'surfaces,' one must conformally map those surfaces onto the plane (the mapping $g : B \to C$ in fig. 4), apply homogenization to the planar configuration C, and, subsequently to determine the composition of the mappings f and g. The deformation gradient associated with the mapping gof serves to carry the homogenized coefficients a_{ij}^h, computed for the graphitic sheet, onto a set of associated homogenized coefficients $\tilde{a}_{ij}^h$ for

the nanotube. While the homogenized coefficients a_{ij}^h should be constants we expect that $\tilde{a}_{ij}^h = \tilde{a}_{ij}^h(x)$. The result of this process may lead to a set of higher-order elastic constants and, thus, to the need for a multipolar theory.

Our work has shown that two classes of results on SWNT shell thickness are prevalent in the literature: *those which assume, a priori, a thickness h equal to the inter-layer separation of graphitic sheets in a graphite crystal and those which are 'backed out' from experimental measurements of in-plane stiffness and flexural rigidity coupled with an assumption of isotropic elastic response.* The in-plane elastic constants in the axial and radial directions for the SWNT, c_{11} and c_{22}, are given by $c_{11} = \tilde{a}_{11}^h$ and $c_{22} = \tilde{a}_{22}^h$ so that the orthotropic constant $\gamma = \tilde{a}_{22}^h/\tilde{a}_{11}^h$; *this constant can be used to compute the in-plane principal bending stiffnesses D_i which is used in place of the flexural rigidity associated with isotropic response to 'back out' a predicted shell thickness h.* Such an approach assumes orthotropic response in the basal plane of a SWNT surface (i.e., $\tilde{a}_{12}^h = \tilde{a}_{21}^h$) as opposed to full anisotropic response. While the principal bending stiffnesses associated with anisotropic response may be computed, *an alternative approach to computing h, which is based on [31]-[34] may also be used.*

The focus of the work in [31]-[34] is the development of an *equivalent continuum model of a representative volume element (RVE) for a nanotube/polymer composite;* as a first step in the formulation of such a model, an atomistic model of the equilibrium response of the graphitic sheet is obtained by employing MD and expressing the total molecular potential energy in the form (15). A transition is then effected which carries the analysis (see fig. 5) from the MD simulation of the energy for the hexagonal array of carbon atoms (5a), to the energy associated with deformation of an 'equivalent' pin-jointed truss (5b), to the strain energy for an 'equivalent' hexagonal plate of thickness h (5c). *Using only the terms, E_R and E_θ, in (15),* the energy for the configuration of fig. 5a was taken in the form

$$E = \sum_a K_a^\rho (\rho_a - P_a)^2 + \sum_a K_a^\theta (\theta_a - \Theta_a)^2 \qquad (18)$$

where P_a and Θ_a refer, respectively, to the undeformed interatomic distance of bond number a and the undeformed bond-angle number a, while ρ_a and θ_a are, respectively, the interatomic distance and bond angle after deformation. The symbols K_a^ρ and K_a^θ stand for the (MD) force constants associated with stretching and angle variance. *The energy (18) ignores the contribution of torsional strain energy.* Using (18) an equivalent continuum model is developed in [32] in a two-step process; first, the hexagonal array of carbon atoms is replaced by a pin-jointed truss model in which truss elements are used to represent the chemical bonds in the lattice structure. In fig. 5b deformations of rods of type a are used to describe bond stretching while stretching and contraction of the rods of type b are used to describe angle variations. The mechanical strain energy for such a truss is

$$\hat{E} = \sum_b \sum_a \frac{A_a^b Y_a^b}{2R_a^b} \left(r_a^b - R_a^b \right)^2 \qquad (19)$$

where A_a^b and Y_a^b are the cross-sectional area and Young's modulus of rod a of truss member type b, respectively, while $r_a^b - R_a^b$ is the 'stretching' of rod a of truss member type b, and R_a^b, r_a^b are the undeformed and deformed lengths, respectively, of the truss elements. *By comparing (18) and (19) the strain energy of the truss model is expressed in terms of the potential energy constants K_a^ρ and K_a^θ.* Finally, the truss model in fig. 5b is replaced by an 'equivalent' continuum plate (fig. 5c); the authors *assume the 'equivalent' plate to be elastically isotropic*

using for its mechanical properties the Young's modulus and Poisson ratio of graphite. It is also assumed that the same amount of elastic strain energy is stored in the two models (truss model (5b) and continuum plate (5c)) when each is deformed under identical static loading conditions; comparison of the strain energies for the models in figs. 5b,c then yields a result for the thickness of the 'equivalent' continuum plate and, therefore, for the effective thickness of the graphitic sheet. The computations in [32] yield effective thicknesses in the range 0.24nm - 0.28nm, *an improvement over the a priori assumption of 0.34nm but not an improvement which resolves the inconsistencies reported in § II.*

In the work we have initiated (i) *the a priori assumption of a strain energy based on isotropic elastic response for the continuum plate (fig. 5c) is replaced by a strain energy based on the constitutive response predicted by homogenization and (ii) the energy E for the atomistic scale hexagon is expanded to include a suitable MD expression for E_ϕ, the torsional strain energy; equivalent energy terms must be incorporated into the total energy for the pin-jointed truss model and then compared, under similar static loading conditions, with the new elastic strain energy expression for the continuum plate so as to yield a prediction of effective thickness;* this will *make possible the computation of a realistic Young's modulus.*

III. REFERENCES CITED

1. C.Q. Ru, 'Effect of van der Waals Forces on Axial Buckling of a Double-Walled Carbon Nanotube,' *J. Appl. Phys.*, 87, (2000), 7227-7231

2. Q. Zhao, M. Nardelli, and J. Bernholc, 'Ultimate Strength of Carbon Nanotubes: A Theoretical Study,' *Phys. Rev. B.*, 65, (2002), 144105-1-144105-5

3. Harris, P.J.F., **Carbon Nanotubes and Related Structures: New Materials for the Twenty-first Century,** Cambridge University Press, (1999), Cambridge, U.K.

4. M.M.J. Treacy, T.W. Ebbsen, and J.M. Gibson, 'Exceptionally High Young's Modulus Observed for Individual Carbon Nanotubes,' *Nature*, 381, (1996), 678-680

5. J.-P. Salvetat, G. Briggs, J-M. Bonnard, R. Basca, A.J. Kulik, T. Stöckli, N. Burnham, and L. Forró, 'Elastic and Shear Moduli of Single-Walled Carbon Nanotube Ropes,' *Phys. Rev. Lett.*, 82, (1999), 944-947

6. D. Qian, C.F. Wagner, W.K. Liu, M.F. Yu, and R.S. Ruoff, 'Mechanics of Carbon Nanotubes,' *Applied Mech. Rev.*, 55, 2002, 495-533

7. O. Lourie, D.M. Cox, and H.D. Wagner, 'Buckling and Collapse of Embedded Carbon Nanotubes,' *Phy. Rev. Lett*, 81, (1998), 1638-1641

8. J.P. Lu, 'Elastic Properties of Carbon Nanotubes and Nanoropes,' *Phy. Rev. Lett.*, 79, (1997), 1297-1300

9. B. Yakobson, C. Brabec, and J. Bernholc, 'Nanomechanics of Carbon Tubes: Instabilities beyond Linear Response,' *Phys. Rev. Lett.*, 76, (1996), 2511-2514

10. S. Govindjec and J. Sackman, 'On the use of Continuum Mechanics to Estimate the Properties of Nanotubes,' *Solid State Communications*, 110, (1999), 227-230

11. C.Q. Ru, 'Effective Bending Stiffness of Carbon Nanotubes,' *Phys. Rev. B.*, 62, (2000), 9973-9975

12. T. Halicioglu, 'Stress Calculations for Carbon Nanotubes' *Thin Solid Films*, 312, (1998), 11-14

13. D. Robertson, D. Brenner, and J. Mintmire, 'Energetics of Nanoscale Graphitic Tubules' *Phys. Rev. B.*, 45, (1992), 12592-12595

14. E. Wong and P. Sheehan, 'Nanobeam Mechanics: Elasticity, Strength, and Toughness of Nanorods and Nanotubes,' *Science*, 277, (1997), 1971-1976

15. C.F. Cornwell and L.T. Wille, 'Elastic Properties of Single-Walled Carbon Nanotubes in Compression,' *Solid State Communications*, 101, (1997), 555-558

16. G. van Lier, C. van Alsenoy, V. van Doren, and P. Geerlings, 'Ab Initio Study of the Elastic Properties of Single-Walled Carbon Nanotubes and Graphene,' *Chem. Phys. Lett.*, 326, (2000), 181-185

17. T. Ozcko, Y. Iwara, and T. Mitani, 'Stiffness of Single-Walled Carbon Nanotubes under Large Strain' *Phys. Rev. Lett*, 84, (2000), 1712-1715

18. N. Yao and V. Lordi, 'Youngs Modulus of Single-Walled Carbon Nanotubes,' *J. Applied Phys.*, 84, (1998), 1939-1943

19. E. Hernández, C. Goze, P. Bernica, and A. Rubio, 'Elastic Properties of C and $B_x C_y N_z$ Composite Nanotubes,' *Phys. Rev. Lett.*, 80, (1998), 4502-4505

20. P. Poncharal, Z. Wang, D. Ugarte, and W.A. de Heer, Electrostatic Deflections and Electromechanical Resonances of Carbon Nanotubes,' *Science*, 283, (1999), 1513-1518

21. M-F. Yu, T. Kowalewski, and R.S.Ruoff, 'Investigation of the Radial Deformability of Individual Carbon Nanotubes under Controlled Indentation Force,' *Phys. Rev. Lett.*, 85, (2002), 1456-1459

22. J-P. Salvetat, J-M. Bonard, A. Kulik, G. Briggs, T. Stöckli, K. Méténier, S. Bonnamy, F. Béguin, N. Burham, and L. Forró, 'Elastic Modulus of Ordered and Disordered Multiwalled Carbon Nanotubes,' *Adv. Mat.*, 11, (1999), 161-165

23. J-P. Salvetat, J.-M. Bonard, N. H. Thompson, A.J. Kulik, L. Forró, W. Benoit, and L. Zuppinoli, 'Mechanical Properties of Carbon Nanotubes,' *Appl. Phys. A.*, 69, (1999), 255-260

24. C.Q. Ru, 'Elastic Buckling of Single-Walled Carbon Nanotube Ropes under High Pressure,' *Phys. Rev. B.*, 62, (2000), 10405-10408

25. C.Q. Ru, 'Column Buckling of Multi-Walled Carbon Nanotubes with Interlayer Radial Displacements,' *Phys. Rev. B.*, 62, (2000), 16962-16967

26. B.T. Kelly, **Physics of Graphite**, Applied Science, (1981), London

27. E. Sanchez-Palencia, **Non-homogeneous Media and Vibration Theory**, Springer-Verlag, 1980 Berlin
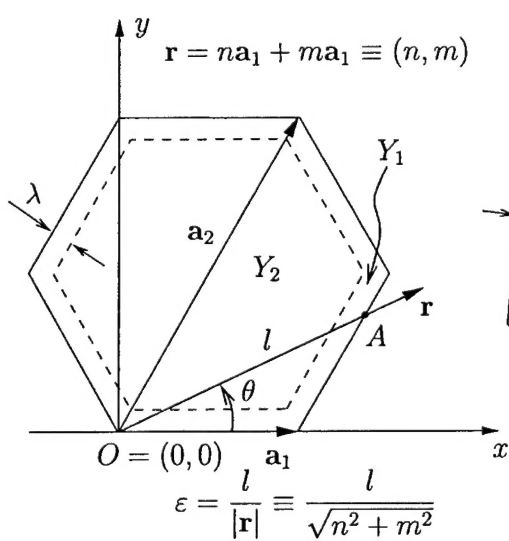
28. A. Bensoussan, J.L. Lions, and G. Papanicoulaou, **Asymptotic Analysis of Periodic Structures**, North Holland, 1978, Amsterdam

29. G. Friesecke and R.D. James, 'A Scheme for the Passage from Atomic to Continuum Theory for Thin films, Nanotubes, and Nanorods,' *J. Mech. Phys. Solids*, 48, (2002), 1519-1540

30. X. Blane, C. Le Bris, and P.C. Lions, 'From Molecular Models to Continuum Mechanics,' *Arch. Rat. Mech. Anal.*, 164, (2002), 341-381

31. T.S. Gates and J.A. Hinkley, 'Computational Materials: Modeling and Simulation of Nanostructured Materials and Systems,' *NASA/TM-2003-21263*, March 2003

32. G.M. Odegard, T.S. Gates, L.M. Nicholson, and K.E. Wise, 'Equivalent-Continuum Modeling of Nano-Structured Materials,' NASA/TM-2001-210863, May 2001

33. G.M. Odegard, T.S. Gates, and K.E. Wise, 'Constitutive Modeling of Nanotube-Reinforced Polymer Composites,' A1AA-2002-1427

34. G.M. Odegard and T.S. Gates, 'Constituve Modeling of Nanotube/Polymer Composites with Various Nanotube Orientations,' 2002 SEM Annual Conference and Exposition on Experimental and Applied Mechanics, June 10-12, 2002 Milwaukee, WI.

35. L.S. Schadler, S.C. Giannaris, and P.M. Ajayan, 'Load Transfer in Carbon Nanotube Epoxy Composites,' *Applied Phys. Lett.*, 73, (1998), 3842-2870

36. D. Qian, E.C. Dickey, R. Andrews, and T. Rantell, 'Load Transfer and Deformation Mechanisms in Carbon Nanotube-Polystyrene Composites,' *Applied Phys. Lett.*, 76, (2000), 2868-2870

37. H. Geng, R. Rosen, B. Zheng, H. Shimoda, L. Heming, J. Liu, and O. Zhou, 'Fabrication and Properties of Composites of Poly(ethylene oxide) and Functionalized Carbon Nanotubes,' *Adv. Mat.* (2003), in press

38. V. Lordi and N. Yao 'Molecular Mechanics of Binding in Carbon-Nanotube Polymer Composites' *J. Mater. Res.*, 15, (2002), 2770-2779

39. H. Bellout, F. Bloom, and J. Nečas, 'Phenomenological Behavior of Multipolar Viscous Fluids,' *Quarterly of Applied Mathematics*, **Vol. L**, (1992), 559-583.

40. H. Bellout, and F. Bloom, 'On the Uniqueness of Plane Poiseulle Solutions of the Equations of Incompressible Bipolar Fluids', *Int. J. Eng. Sciences,* **31**, (1993), 1535-1549.

41. H. Bellout and F. Bloom, 'Steady Plane Poiseulle Flows of Incompressible Multipolar Fluids,' *Int. J. Nonlinear Mech.*, 23, (1993), 503-518.

42. H. Bellout, F. Bloom, and J. Nečas, 'Existence, Uniqueness, and Stability of Solutions to the Initial Boundary-Value Problem for Bipolar Viscous Fluids,' *Differential and Integral Equations*, (1995), 453-464.

43. H. Bellout, F. Bloom, and J. Nečas, 'Bounds for the Dimensions of the Attractors of Nonlinear Bipolar Viscous Fluids,' *Asymptotic Analysis*, 11, (1995), 1-37.

44. F. Bloom and W. Hao, 'Steady Flows of Nonlinear Bipolar Viscous Fluids Between Rotating Cylinders.' *Quarterly of Applied Mathematics*, **Vol. LIII**, (1995), 143-171.

45. J. Tersoff and R.S. Ruoff, 'Structural Properties of a Carbon-Nanotube Crystal,' *Phys. Rev. Lett.*, 73, (1994), 676-679

46. H. Bellout and F. Bloom, 'Modelling the Buckling of Rectilinearly Orthotropic Truncated Conical Shells,' *Math. Comput. Modelling*, 34, (2001), 195-227

47. T. Ozaki, Y. Iwasa, and T. Mitani, 'Stiffness of Single-Walled Carbon Nanotubes under Large Strain,' *Phys. Rev. Lett.*, 84, (2000), 1712-1715

48. F. Bloom and D.W. Coffin, **Handbook of Thin Plate Buckling and Postbuckling**, CRC Press, (2000), Boca Raton, FL.
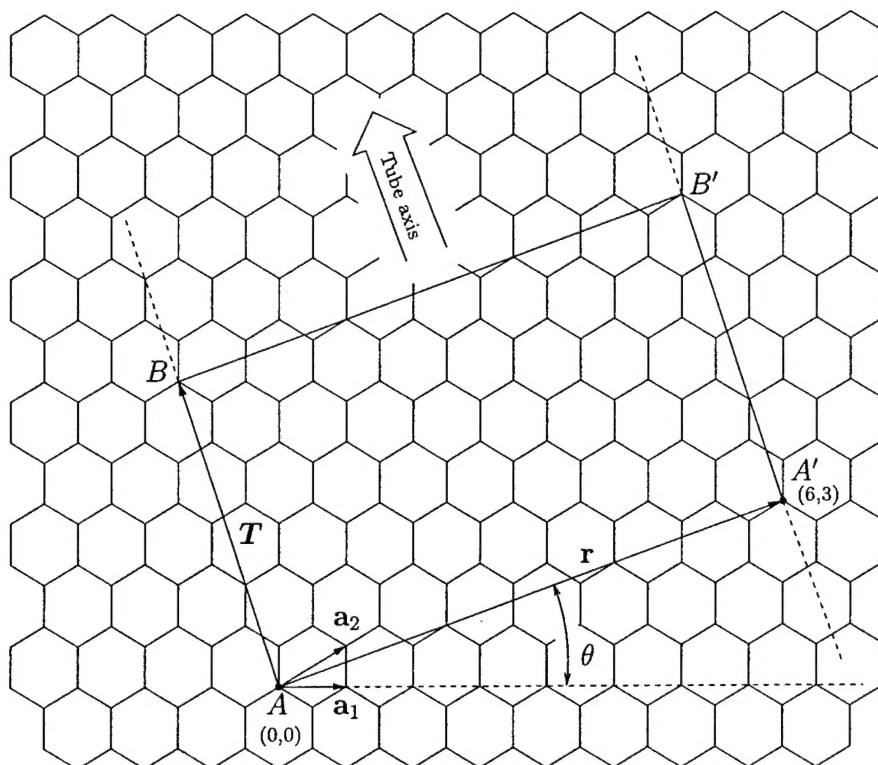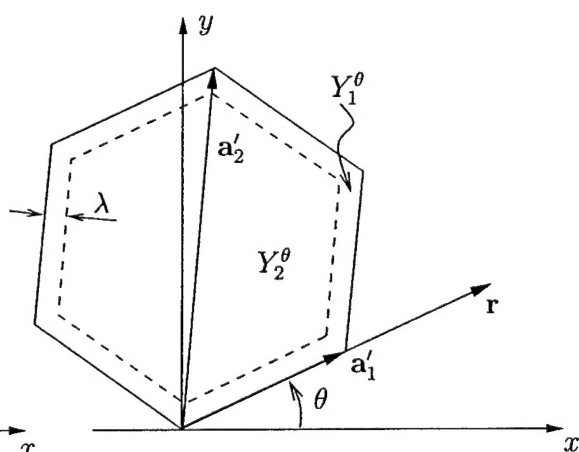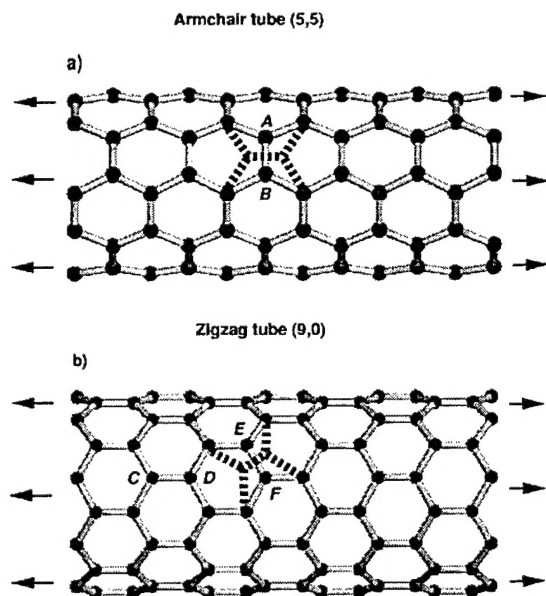
Figure 1 (from P.J.F. Harris, Carbon Nanotubes and Related Structures, New Materials for the Twenty-First Century, Cambridge University Press, 2003, Cambridge, U.K.)
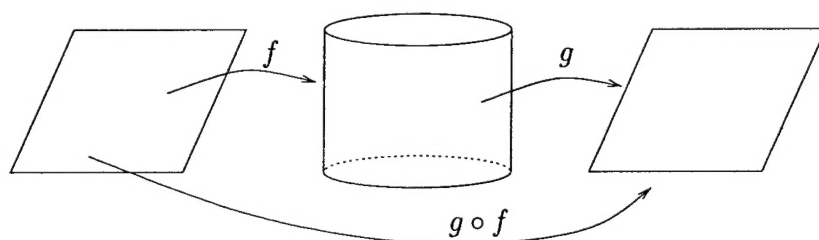

$$\mathbf{r} = n\mathbf{a_1} + m\mathbf{a_1} \equiv (n, m)$$

$$\varepsilon = \frac{l}{|\mathbf{r}|} \equiv \frac{l}{\sqrt{n^2 + m^2}}$$

Figure 2a.

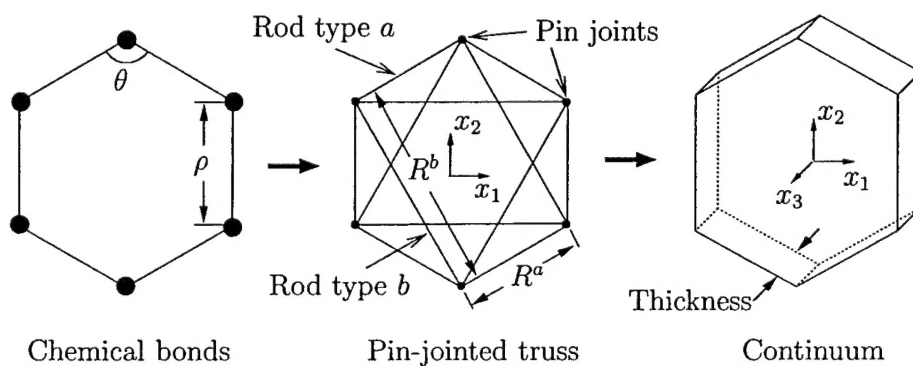**Figure 2b.**

Armchair tube (5,5)

a)

Zigzag tube (9,0)

b)

Figure 3. (from Q. Zhao, M. Nardelli, & J. Bernholc, 'Ultimate Strength
of Carbon Nanotubes: A Theoretical Study,' Phys. Rev. B. 65,
(2002), 144105-1-144103).

Figure 4.

Chemical bonds   Pin-jointed truss   Continuum

Figure 5. (from T.S. Gates & J.A. Hinkley, 'Computational Materials: Modeling
and Simulation of Nanostructured Materials and Systems', NASA/TM-
2003-212103, NASA Langley Research Center, Hampton, VA)